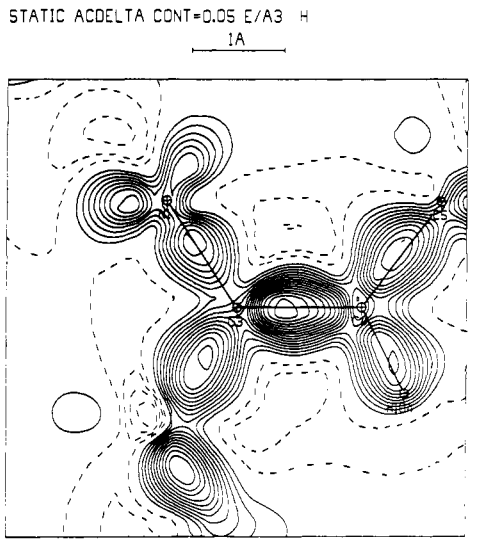

Figure 13. Crystallographic static deformation density in the plane defined by the atoms C_α–C_β–N_1. Contours as in Figure 2.

jugation Scheme 2. Anyhow the difference of reactivity between peptides and α,β-dehydrogenated pseudopeptides is certainly more related to the special molecular conformation of the side chain imposed by the C_α=C_β double bond rather than to electronic effects. Very recent results of Souhassou and Li[48] indicate that whereas the α,β-dehydrogenation and conjugation effects are not visible in the deformation density maps, the effects can be seen clearly in a topological analysis of the gradient vector paths and the Laplacian of the total electron density using the methods of Bader and his co-workers.[49]

Acknowledgment. Support of this work by the CNRS and the University of Nancy I is gratefully acknowledged. We thank Dr. A. Aubry for fruitful discussions, and Drs. G. Boussard and M. Marraud for the generous gift of this α,β-dehydropeptide. R.H.B is grateful for support from USDHHS PHS NIH Grant GM34073. The quantum-chemical calculations were carried out with a grant for computing time of the CNRS on the IBM 30-90 of "Le centre de calcul de Strasbourg Cronenbourg"; the staff is gratefully acknowledged for this collaboration.

Registry No. *N*-AcΔPhe-NHMe, 81307-03-1.

Supplementary Material Available: Residual density maps in the C_α=C_β plane, in the N_2—C′=O_1 plane, in the benzene group, and in the N_1—C′—O_0 plane at 1.35- and 0.90-Å^{-1} resolution and deformation density maps of the benzene group and of the C_α=C_β double bond at 1.0-Å^{-1} resolution (3 pages); listing of observed and calculated structure factors and esd's (39 pages). Ordering information is given on any current masthead page.

(48) Souhassou, M.; Li, N. *American Crystallographic Meeting*, Toledo, OH, July 1991.
(49) Bader, R. F. W. *Atoms in Molecules—A Quantum Theory*; Oxford Union Press: Oxford, UK, 1990.

Theoretical Studies of the Kinetics, Thermochemistry, and Mechanism of H-Abstraction from Methanol and Ethanol

Leonardo Pardo,† Jason R. Banfelder, and Roman Osman*

Contribution from the Department of Physiology and Biophysics, Mount Sinai School of Medicine of the City University of New York, One Gustave L. Levy Place, New York, New York 10029. *Received March 4, 1991*

Abstract: The process of hydrogen abstraction from methanol and ethanol has been calculated with ab initio quantum chemical methods with extended basis sets (6-311G**) and with the inclusion of correlation up to MP4SDQ. These studies serve as a model of such processes in large molecules of biological importance including the sugar moiety of DNA. A comparison of geometries of ground and transition states optimized at UHF and MP2 levels with the 6-31G basis set shows that the UHF optimized geometries have lower energies at the highest level of theory used (MP4SDQ/6-311G**). The transition states occur at a somewhat later stage along the reaction coordinate at the UHF level than at the MP2 level. Energy barriers, along with zero-point energies, were used to calculate the rate constants for H-abstraction from C_α of methanol and ethanol. Tunneling corrections were applied according to an Eckart treatment of an unsymmetrical unidimensional barrier. The corrected rate constants are in very good agreement with experiment over a wide range of temperatures. The same approach was used to predict the rate constant for the abstraction of the hydrogen from C_β of ethanol, which is not known from experimental measurements. The calculated C–H bond strengths and heats of reactions are also in good agreement when the correlation energy is scaled according to the MPnSAC approach. The geometric and energetic parameters of the transition states behave according to Hammond's postulate, i.e., the more exothermic the H-abstraction, the closer is the transition state to the reactants. This relationship suggests that the C–H bond strength is one of the major factors that determine the barrier to H-abstraction. An analysis of the MCSCF wave function constructed from a CAS of three electrons distributed in three orbitals (σ_{CH}, σ^*_{CH}, and the orbital containing the unpaired electron) supports this conclusion.

Introduction

The severe biological consequences of exposure to ionizing radiation are attributable to the lesions it causes in essential biological molecules. DNA is one of the most important target molecules that is damaged as a result of the chemical reactions caused by ionizing radiation, because irreparable damage produced in DNA usually leads to cell death. Hydroxyl radicals (OH•) produced by ionizing radiation can lesion DNA by an indirect mechanism of hydrogen abstraction, which is followed by a β-elimination of the phosphate to produce a strand break.[1] The hydrogen abstraction from deoxyribose seems to be the critical

† Permanent address: Laboratory of Computational Medicine, Department of Biostatistics, Faculty of Medicine, Universidad Autonoma de Barcelona, 08193 Bellaterra, Barcelona, Spain.

(1) von Sonntag, C. *The Chemical Basis of Radiation Biology*; Taylor & Francis: London, 1987.

0002-7863/92/1514-2382$03.00/0

step in this process because it leads to a strand break and ultimately to reproductive cell death.[2-4]

In order to understand the process of H-abstraction in deoxyribose, we have chosen to investigate this process in methanol and ethanol for which the barriers and the rate constants for H-abstraction were determined experimentally in the gas phase.[5-9] High-quality quantum chemical calculation of H-abstraction reactions by OH• have been performed before, but they were limited to H_2[10] or CH_4.[11-15] The theoretical approaches taken in those studies include large-scale POL-CI,[10] MCHF/CI,[15] UHF/CI,[14] as well as Møller–Plesset many-body perturbation techniques[11,12] with extended basis sets. In a recent work, Truong and Truhlar[11] calculated the reaction rate constant for H-abstraction from methane by OH• using transition state theory and an Eckart model for tunneling correction. They showed that the calculated rate constants are in good agreement with experimental data.

In the present work we report on the ab initio quantum chemical simulations of the process of H-abstraction from methanol and ethanol. A comparison between computed and measured values for this fundamental chemical process shows that kinetic parameters obtained from high quality quantum chemical calculations are in good agreement with experimental values. Using the same methods, we predict the rate constant for the abstraction of the H_β of ethanol over a range of temperatures. An experimental study of the kinetics of this process has not been reported. We also show that the strength of the C–H bond is one of the important parameters in determining the susceptibility for the abstraction of a specific hydrogen.

Methods

All the quantum mechanical calculations were performed with ab initio methods in the GAUSSIAN 86[16] or HONDO[17] systems of programs.

A. Geometries and Electronic Structure. The simulations of hydrogen abstraction by a hydroxyl radical include structure optimizations of reactants and transition states (TS). The structure optimizations were performed with the 6-31G basis set both at the level of unrestricted Hartree–Fock (UHF) and with second-order Møller–Plesset perturbation theory (MP2).[18] An optimization at the MP2 level requires the inclusion of all the orbitals in the calculation of the second-order correction to the energy expression. Thus, all the calculations of the correlation energy with the Møller–Plesset technique included all the orbitals. The systems studied in this work are composed of a closed shell molecule interacting with a radical (e.g., alcohol and OH• or water and alcohol radical). As doublets, the expectation value of the spin operator S^2 should be 0.75; in the UHF calculations presented here this value did not exceed 0.796.

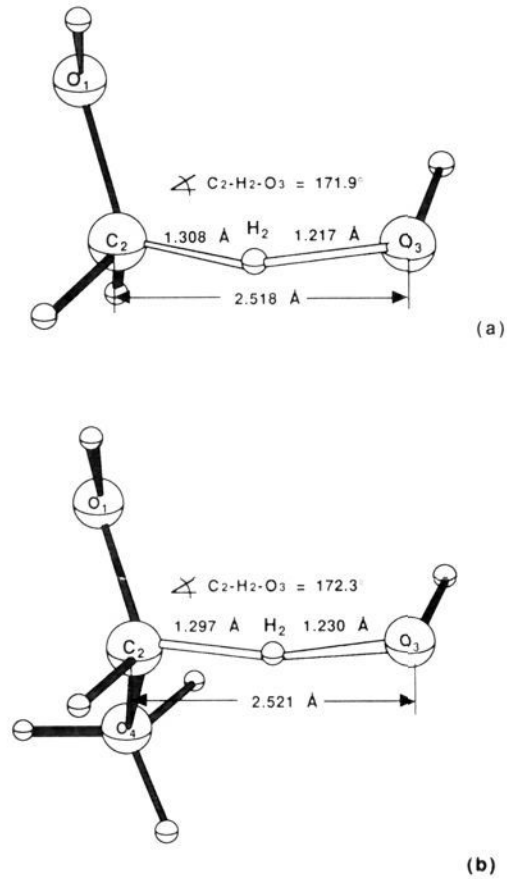

Figure 1. Structures of transition states for H_α-abstraction by OH•: (a) abstraction from methanol; (b) abstraction from ethanol.

The approximate position of the TS at the UHF/6-31G level was located by calculating a limited portion of the potential energy surface using the C_2–O_3 and C_2–H_2 distances in the $CH_3OH\cdots OH^\bullet$ complex as reaction coordinates (see Figure 1 for notation of atoms). These approximate structures were used as an initial guess for a full optimization of the TS. The structures found have the characteristic of a transition state, with a single negative eigenvalue in the matrix of force constants. The major contribution to the corresponding eigenvector comes from the internal coordinates associated with stretching the C_2–H_2 and C_2–O_3 bonds. The structures of the TS were also fully optimized at the MP2/6-31G level starting from the structural parameters and force constants obtained from the optimization at the UHF/6-31G level. The major contribution to the corresponding eigenvector comes from the same internal coordinates.

Electron correlation energy was calculated up to fourth-order Møller–Plesset perturbation theory in the space of single, double, and quadruple excitations (MP4SDQ) from all the molecular orbitals (see above). The basis sets for these calculations were chosen from those incorporated in the GAUSSIAN 86 package and they included the split valence 6-31G, the split valence augmented with polarization functions on heavy atoms, 6-31G*, and the valence triple zeta (ζ) plus polarization on all atoms, 6-311G**.[16]

The electronic structure of the reactants and the TS that are relevant to the process of hydrogen abstraction were calculated with the multiconfigurational SCF (MCSCF) method with the 6-31G basis set. The active space of the MCSCF calculations included three electrons in three orbitals. In the reactants, the active space consisted of the C–H bond that is broken in the process of H-abstraction, the orbital with the unpaired electron localized on the oxygen of the hydroxyl radical, and of the C–H antibonding orbital. The same orbitals were used in the MCSCF calculations of the TS. Three electrons, distributed in all possible ways in three orbitals within the given multiplicity (doublet), yield eight configurations which were optimized with the MCSCF procedure. All one-electron properties, such as Mulliken populations and spin densities, were calculated from the MCSCF/6-31G wave function.

B. Energetics of H-Abstraction. For all processes considered, the energy of reaction, ΔV_{react}, is defined as the sum of the energies of all products minus the sum of the energies of all reactants. The energy of activation, $\Delta V^\ddagger$, is defined as the energy of the TS minus the sum of the

(2) Lloyd, D. C. *Int. J. Radiat. Biol.* **1985**, *48*, 940–942.
(3) Roberts, C. J.; Holt, P. D. *Int. J. Radiat. Biol.* **1985**, *48*, 927–939.
(4) Radford, I. R. *Int. J. Radiat. Biol.* **1985**, *48*, 45–54.
(5) Meier, U.; Grotheer, H. H.; Riekert, G.; Just, T. *Ber. Bunsenges. Phys. Chem.* **1985**, *89*, 325–327.
(6) Atkinson, R. *Int. J. Chem. Kinet.* **1987**, *19*, 799–828.
(7) Pagsberg, P.; Munk, J.; Sillesen, A.; Anastasi, C. *Chem. Phys. Lett.* **1988**, *146*, 375–381.
(8) Hess, W. P.; Tully, F. P. *J. Phys. Chem.* **1989**, *93*, 1944–1947.
(9) Wallington, T. J.; Kurylo, M. J. *Int. J. Chem. Kinet.* **1987**, *19*, 1015–1023.
(10) Walch, S. P.; Dunning, T. H., Jr. *J. Chem. Phys.* **1980**, *72*, 1303–1311.
(11) Truong, T. N.; Truhlar, D. G. *J. Chem. Phys.* **1990**, *93*, 1761–1769.
(12) Gordon, M. S.; Truhlar, D. G. *J. Am. Chem. Soc.* **1986**, *108*, 5412–5419.
(13) Dunning, T. H., Jr.; Harding, L. B.; Bair, R. A.; Eades, R. A.; Shepard, R. L. *J. Phys. Chem.* **1986**, *90*, 344–356.
(14) Sana, M.; Leroy, G.; Villaveces, J. L. *Theor. Chim. Acta* **1984**, *65*, 109–125.
(15) Dupuis, M.; Lester, W. A., Jr. *J. Chem. Phys.* **1984**, *81*, 847–850.
(16) Frisch, M. J.; Binkley, J. S.; Schlegel, H. B.; Raghavachari, K.; Melius, C. F.; Martin, R. L.; Stewart, J. J. P.; Bobrowicz, F. W.; Rohlfing, C. M.; Kahn, L. R.; Defrees, D. J.; Seeger, R.; Whiteside, R. A.; Fox, D. J.; E. M., F.; Pople, J. A. *Gaussian 86*; Gaussian, Inc.: Pittsburgh, PA, 1986.
(17) Dupuis, M.; Watta, J. D.; Villar, H. O.; Hurst, G. J. B. *HONDO*; IBM; Kingston, NY, 1988.
(18) Hehre, W. J.; Radom, L.; Schleyer, P. v. R.; Pople, J. A. *Ab Initio Molecular Orbital Tehroy*; John Wiley: New York, 1986.

energies of all reactants. The superscript "f" indicates that this is the barrier for the forward reaction; the barrier for the reverse reaction is given a superscript "r".

The zero-point vibrational energy (ZPE) was calculated for each stationary point found. Those barriers that include ZPE corrections are given a subscript "c"; those that do not are given a subscript "u".

To calculate the enthalpy of reaction, ΔH_{react}, we follow the method of Pople et al.[19] Because the process under consideration is a gas-phase reaction in which the number of molecules does not change, it is assumed that at absolute zero the enthalpy of reaction is equal to the energy of the reaction. Thermal corrections are applied to obtain the enthalpy of reaction at 298.15 K, ΔH_{react}, according to the following equation:

$$\Delta H_{react} = \Delta V_{react} + [H°(298) - H°(0)]_{products} - [H°(298) - H°(0)]_{reactants} \quad (1)$$

where the thermal corrections, $[H°(298) - H°(0)]$, are calculated from normal mode vibrational frequencies.

C. Calculation of Rate Constants and Tunneling Correction. The second-order rate constant expressed in units of volume per mole per unit time is given by the following equation:

$$k(T) = \frac{k_b T}{h} \frac{q_{TS}}{q_{OH} \cdot q_{ROH}} \exp(-\Delta V_c^f / RT) \quad (2)$$

where k_b is Boltzman's constant, T is temperature, h is Planck's constant, and the q's are the molecular partition functions for the indicated molecules (OH• or ROH) or the TS complex. The molecular partition functions can be written as the product of translational, electronic, vibrational, and rotational partition functions. A few details relating to the vibrational components of partition functions are worth mentioning. In particular, in evaluating q_{TS}, the term corresponding to motion over the col (i.e., the term involving the imaginary frequency) is considered as a translational motion in one dimension and is therefore omitted from the evaluation of the vibrational partition function of the TS. Also, the internal (hindered) rotations are treated as harmonic vibrations. As demonstrated in a recent study,[11] this approximation reduces the calculated rate constant by a factor that ranges from 1.5 at 200 K to 4.7 at 2000 K.

Tunneling correction to the rate constant was calculated by the zero-order approximation to the vibrationally adiabatic potential energy surface model with zero curvature.[11] In this approximation the tunneling is assumed to occur along a unidimensional minimum energy path. The potential energy curve is approximated by an unsymmetrical Eckart potential energy barrier[20] that is required to go through the zero-point-corrected energies of the reactants, transition state, and products. The equations that describe the Eckart potential energy function are adapted from Truong and Truhlar.[11]

The Eckart potential function is described by

$$V = -\frac{ay}{1-y} - \frac{by}{(1-y)^2} \quad (3)$$

where

$$y = -e^{\lambda x} \quad (4)$$

and the range parameter, λ, is defined by

$$\lambda^2 = -\frac{\mu(v^*)^2 B}{2\Delta V_u^f(\Delta V_u^f - A)} \quad (5)$$

where μ is the reduced mass and v^* is the imaginary frequency at the transition state. The constants a, b, A, and B are defined below.

Solving the Schroedinger equation for the Eckart function yields the transmission probability

$$\kappa(E) = 1 - \frac{\cosh[2\pi(\alpha - \beta)] + \cosh[2\pi\delta]}{\cosh[2\pi(\alpha + \beta)] + \cosh[2\pi\delta]} \quad (6)$$

where

$$\alpha = \frac{1}{2}\sqrt{\frac{E}{C}} \quad (7)$$

$$\beta = \frac{1}{2}\sqrt{\frac{E-a}{C}} \quad (8)$$

$$\delta = \frac{1}{2}\sqrt{\frac{b-C}{C}} \quad (9)$$

$$C = \frac{(hv^*)^2 B}{16\Delta V_u^f(\Delta V_u^f - A)} \quad (10)$$

$$A = \Delta V_u^f - \Delta V_u^r \quad (11)$$

$$B = 2\Delta V_u^f - A + 2\sqrt{\Delta V_u^f(\Delta V_u^f - A)} \quad (12)$$

$$a = \Delta V_c^f - \Delta V_c^r \quad (13)$$

$$b = 2\Delta V_c^f - a + 2\sqrt{\Delta V_c^f(\Delta V_c^f - a)} \quad (14)$$

The tunneling correction, Γ^*, is obtained as the ratio between the quantum mechanical and the classical rate constants calculated by integrating the respective transmission probabilities over all possible energies.

$$\Gamma^*(T) = \frac{e^{\Delta V_c^f}}{kT} \int_0^\infty e^{-E/kT} \kappa(E)\, dE \quad (15)$$

The integral is evaluated numerically using Mathematica running on a SUN 386i.[21]

Results and Discussion

The reactions of OH radical with methanol and ethanol have been studied using discharge flow/laser fluorescence techniques. Experimentally measured rate cosntants for H_α-abstraction from methanol and ethanol were determined in the gas phase over a range of temperatures.[5-9,22-24] These experimental data can be used to calibrate the level of theoretical methods needed to adequately describe such reactions, and their extensions to systems where experimental results are not available.

A. Potential Energy Surface of Hydrogen Abstraction: Optimized Structures. 1. Structures of Reactants and Products. Hydrogen abstraction by hydroxyl radical from methanol produces primarily the hydroxymethyl radical ($•CH_2OH$) with the radical on the α-carbon. The abstraction of the hydroxyl hydrogen is slower and less prevalent and the $CH_3O•$ is produced only in small quantities. At 300 K the contribution of the $CH_3O•$ is estimated to be approximately 15%.[24] In ethanol, two different types of carbon-bound hydrogens can be abstracted by hydroxyl radical: the abstraction of hydrogens bonded to an α-carbon (α-abstraction) produces the α-hydroxyethyl radical ($•CH(CH_3)OH$) and the abstraction of hydrogens bonded to a β-carbon yields the β-hydroxyethyl radical ($•CH_2CH_2OH$). The β-hydroxyethyl radical can also be obtained from the addition of an OH• to ethylene. Structure optimization of methanol and ethanol and their α-radicals at the UHF and MP2 level with the 6-31G basis set yields structures that are virtually identical with those obtained in other theoretical studies.[18,25] The structures are also in agreement with experimental values.[26] The minimum energy structure of $•CH_2OH$ obtained in the present work is equivalent to the one with C_1 geometry described in the work by Saebo et al.,[27] in which the rotation–inversion potential energy hypersurface of $•CH_2OH$ was studied. The structure of the $•CH(CH_3)OH$ radical around the α-carbon is almost identical with that of the $•CH_2OH$ structure. The optimized C_α–C_β bond length in the α-hydroxyethyl radical is 1.4878 Å, and the methyl is in a nearly perfectly staggered conformation with respect to the oxygen atom. The dihedral angles of the three methyl hydrogens are 66.4°, 186.8°, and 307.0°. The structure of the β-hydroxyethyl radical was only optimized at the UHF/6-31G level. The structural parameters obtained are in agreement with the structure obtained

(19) Pople, J. A.; Luke, B. T.; Frisch, M. J.; Binkley, J. S. *J. Phys. Chem.* **1985**, *89*, 2198–2203.
(20) Eckart, C. *Phys. Rev.* **1930**, *35*, 1303.
(21) Wolfram, S.; Grayson, D.; Maeder, R.; Cejtin, H.; Gray, T.; Omohundro, S.; Ballman, D.; Keiper, J. *Mathematica: A System for Doing Mathematics by Computer*; Wolfram Research Inc.: New York, 1988.
(22) Overend, R.; Paraskevopoulos, G. *J. Phys. Chem.* **1978**, *82*, 1329.
(23) Meier, U.; Grotheer, H. H.; Riekert, G.; Just, T. *Chem. Phys. Lett.* **1985**, *115*, 221.
(24) Atkinson, R. *Chem. Rev.* **1985**, 69–201.
(25) Yates, B. F.; Bouma, W. J.; Radom, L. *J. Am. Chem. Soc.* **1987**, *109*, 2250.
(26) Kohata, K.; Fukuyama, T.; Kuchitsu, J. *J. Phys. Chem.* **1982**, *86*, 602.
(27) Saebo, S.; Radom, L.; Schaefer, H. F., III *J. Chem. Phys.* **1983**, *78*, 845–853.

Table I. Total Energies (hartrees) and Zero-Point Energies (kcal/mol, in Parentheses) for Reactants and Products in Hydrogen Abstraction Reactions from Alcohols

	optimization level								
	HF/6-31G					MP2/6-31G			
	HF/ 6-31G	HF/ 6-31G*	MP2/ 6-31G*	HF/ 6-311G**	MP4/ 6-311G**	MP2/ 6-31G	HF/ 6-311G**	MP4/ 6-311G**	ΔE^a
				Reactants					
CH_3OH	−114.988 16 (34.44)	−115.034 13	−115.351 55	−115.074 40	−115.495 14	−115.206 35 (32.42)	−115.070 66	−115.494 30	0.53
CH_3CH_2OH	−154.013 23 (53.82)	−154.074 43	−154.527 05	−154.124 31	−154.727 04	−154.323 05 (50.86)	−154.120 11	−154.726 19	0.54
OH	−75.363 18 (5.47)	−75.382 20	−75.523 07	−75.410 49	−75.604 49	−75.452 72 (5.08)	−75.409 24	−75.604 01	0.30
				Products					
CH_2OH	−114.362 93 (24.71)	−114.407 20	−114.701 35	−114.447 26	−114.835 49	−114.560 98 (23.55)	−114.444 64	−114.834 95	0.34
CH_3CHOH	−153.391 20 (44.29)	−153.450 53	−153.879 10	−153.499 41	−154.068 91	−153.679 85 (42.14)	−153.496 34	−154.068 40	0.32
CH_2CH_2OH	−153.382 84 (43.69)	−153.441 89	−153.866 83	−153.491 13	−154.057 58				
H_2O	−75.985 36 (14.11)	−76.009 68	−76.197 32	−76.045 81	−76.288 66	−76.114 21 (13.09)	−76.044 07	−76.288 62	0.03

[a] ΔE (kcal/mol) is defined as the difference between the MP4SDQ/6-311G** total energies of the structures optimized at the MP2/6-31G and HF/6-31G level, respectively.

Table II. Selected Structural Parameters and Total Energies of Transition States in the H-Abstraction Process Calculated from the HF/6-31G and MP2/6-31G (in Parentheses) Optimized Geometries

		ethanol		
	methanol	α-H	β^{I}-H	β^{II}-H
		Structural Parameters[a]		
C_2–O_3	2.518 (2.516)	2.521 (2.523)	2.487[b]	2.509[b]
C_2–H_2	1.308 (1.235)	1.297 (1.224)	1.339[c]	1.310[c]
O_3–H_2	1.217 (1.300)	1.230 (1.322)	1.182[d]	1.221[d]
O_1–C_2–H_2	109.6 (110.4)	108.1 (108.7)	105.3[e]	101.9[e]
O_1–C_2–O_3	105.8 (103.0)	104.5 (101.1)	97.8[f]	95.5[f]
C_2–H_2–O_3	171.9 (165.5)	172.3 (164.6)	161.4[g]	164.7[g]
H–O_1–C_2–H_2	−70.7 (−69.4)	−69.0 (−69.4)	52.4[h]	57.8[h]
O_1···H···O_3			122.1[i]	125.6[j]
		Total Energies (hartrees)		
HF/6-31G//HF/6-31G	−190.308 78	−229.336 65	−229.333 79	−229.333 30
HF/6-311G**//HF/6-31G	−190.447 45	−229.499 64		
MP4/6-311G**//HF/6-31G	−191.093 13	−230.328 06		
HF/6-31G*//HF/6-31G	−190.374 33	−229.417 14	−229.412 19	−229.413 48
MP2/6-31G*//HF/6-31G	−190.867 13	−230.046 23	−230.039 66	−230.040 88
MP2/6-31G//MP2/6-31G	−190.640 30	−229.760 25		
HF/6-311G**/MP2/6-31G	−190.444 77	−229.496 81		
MP4/6-311G**//MP2/6-31G	−191.087 37	−230.321 84		
ΔE (kcal mol^{-1})[k]	3.62	3.90		
		Zero-Point Energies (kcal mol^{-1})		
HF/6-31G	38.28	57.46	57.87	57.84
MP2/6-31G	36.15	54.45		

[a] Bond distances in Å and angles in deg; see Figures 1 and 2 for notation of atoms. [b] C_4–O_3. [c] C_4–H_4. [d] O_3–H_4. [e] C_2–C_4–H_4. [f] C_2–C_4–O_3. [g] C_4–H_4–O_3. [h] O_1–C_2–C_4–H_4. [i] O_1···H–O_3. [j] O_1–H···O_3. [k] ΔE as defined in text and in Table I.

by Sosa et al.[28] as part of their study of the addition of hydroxyl radical to ethylene.

Table I shows the total energies obtained for the reactants and products at different levels of theory. In order to evaluate the quality of the optimized geometries obtained at UHF and MP2 levels, single point calculations were done with the MP4SDQ/6-311G** method. The last column of Table I (ΔE) shows the difference between the total energy at the MP4SDQ/6-311G** level of geometries optimized at the MP2/6-31G and the HF/6-31G level, respectively. As can be seen from Table I, at the MP4SDQ/6-311G** level, the optimized geometries at the HF level give consistently lower energies than those optimized at the MP2 level. These results reflect the fact that the optimized structure is a function of the level of calculation. In particular, inclusion of electron correlation at the MP2 level for structure optimization seems to yield geometries that are further away from the ideal "MP4 geometries" than those optimized at the HF level. Thus, inclusion of partial electron correlation, as in MP2, may contribute to a more distorted geometry than an optimization at the HF level.

2. Structures of Transition States. The process of hydrogen abstraction by hydroxyl radical can be considered as a collision event. The hydroxyl radical approaches a C–H bond with its unpaired electron and upon contact forms an O–H bond while the original C–H bond is homolytically broken. The structures of the TS for H_α abstraction of methanol and ethanol at the UHF/6-31G level are depicted in Figue 1, a and b. Structural parameters and total energies at different levels of theory are shown in Table II.

A comparison of the structural parameters of the TS that result from optimizations at different computational levels (UHF versus MP2, Table II) reveals an important difference. While the distance of approach of the hydroxyl radical to the carbon bearing the abstracted hydrogen (C_2–O_3) is virtually the same at both

(28) Sosa, C.; Schlegel, B. *J. Am. Chem. Soc.* **1987**, *109*, 4193–4198.

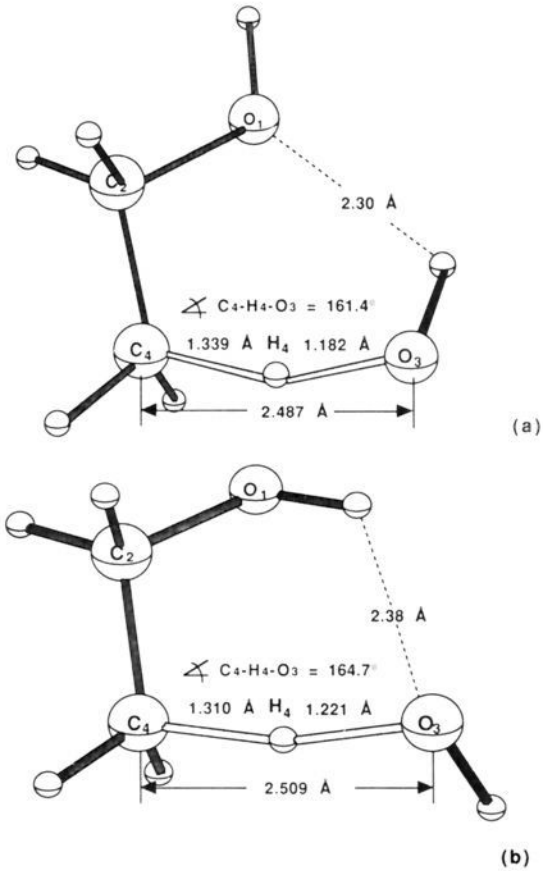

Figure 2. Structures of transition states for H_β-abstraction by OH• from ethanol demonstrating the intramolecular hydrogen bonding: (a) structure β^{I}; (b) structure β^{II}.

levels, the UHF optimization yields a structure in which the C_2–H_2 bond is longer by 0.073 Å than the one obtained from the MP2 optimization. Similarly, the O_3–H_2 bond that is formed is shorter by 0.083 Å in the UHF than in the MP2 optimization. Thus, the UHF optimization yields a somewhat later TS with a structure closer to the products. A comparison of the MP4/6-311G** energies of the transition states optimized with UHF/6-31G and MP2/6-31G theory shows that the UHF structure has a lower energy. However, because a transition state does not represent a variational structure with respect to all the internal coordinates, one may not conclude that the UHF optimized TS is necessarily a better structure. The MP2 optimizations produce better frequencies, especially of the imaginary frequency at the TS, where a reduction of 25–28% is observed (see Table III). Since these results do not point unequivocally to which optimization method is better, we decided to rely on the results from the calculation of the rate constants (see below), which indicate that an optimization at the UHF/6-31G level gives good results. Thus, the TS for the hydrogen abstraction reaction from C_β of ethanol has been only optimized at the UHF/6-31G level. Two transition states have been identified and they have been designated as β^{I} and β^{II}. The structural parameters and total energies of the two TS are listed in Table II; their structures are shown in Figure 2, a and b. In the β^{I} structure (Figure 2a), the OH• functions as a hydrogen donor in the hydrogen bond to O_1, whereas in the β^{II} structure (Figure 2b), it serves as a hydrogen acceptor in the hydrogen bond from O_1. The latter structure has a lower energy at the MP2/6-31G* level and was therefore selected as the TS for which the rate constant was calculated.

Analysis of the structural parameters of the TS structures of H-abstraction shows that the two internal coordinates that contribute to the reaction coordinate (the major components of the eigenvector of the Hessian matrix with the negative eigenvalue) are inversely correlated. The C–O distance for H_α-abstraction

Table III. Kinetic Parameters and Tunneling Corrections for H-Abstraction from Methanol and Ethanol

	methanol[a,c] α-H				ethanol[b,c]				ethanol[d]
calculation level basis set optimization level	MP2 6-31G* HF/6-31G	MP4 6-311G** HF/6-31G	MP4 6-311G** MP2/6-31G	MP4-SAC 6-311G** MP2/6-31G	MP2 6-31G* HF/6-31G	MP4 6-311G** HF/6-31G	MP4-SAC 6-311G** MP2/6-31G	MP2 6-31G* HF/6-31G
barriers (kcal mol^{-1})								
ΔV_u^t	4.70	4.08	6.86	4.08	2.44	2.18	2.46	5.80
ΔV_c^t	3.07	2.45	5.51	2.73	0.61	0.35	0.98	4.35
ΔV_u^r	19.79	19.46	22.72	21.82	18.94	18.52	21.11	14.60
ΔV_c^r	19.25	18.92	22.22	21.33	18.00	17.58	20.33	14.64
imaginary freq (cm^{-1})								
$-i\nu$	3071.3	3071.3	2351.4	2351.4	2995.8	2995.8	2160.6	2987.0
tunneling corr								
Γ^*	18.895	10.738	45.853	8.809	1.448	1.047	2.012	58.204
rate constants × 10^{12} (cm^3 molecule^{-1} s^{-1})								
k(TSTSYM)	1.27×10^{-2}	3.68×10^{-2}	2.17×10^{-4}	2.55×10^{-2}	4.08×10^{-1}	6.37×10^{-1}	2.50×10^{-1}	5.08×10^{-4}
k(TSTSYM/ZCG-O)	2.40×10^{-1}	3.95×10^{-1}	9.95×10^{-3}	2.25×10^{-1}	5.91×10^{-1}	6.67×10^{-1}	5.03×10^{-1}	2.96×10^{-2}
k(exp)		9.34×10^{-1}				3.27		

[a] Temperature-dependent values at 294 K.[8] [b] Temperature-dependent values at 293 K.[31] [c] Abstracted atom α-H. [d] Abstracted atom β^{II}-H.

Table IV. Rate Constants of H-Abstraction (cm^3 $molecule^{-1}$ s^{-1}) from Methanol and Ethanol as a Function of Temperature (K)

	methanol		ethanol H_α		ethanol H_β
temp	calcd MP4/6-311G**//HF/6-31G	exptl[a]	calcd MP4/6-311G**//HF/6-31G	exptl[b]	calcd MP2/6-31G*//HF/6-31G
200	2.74×10^{-13}	5.357×10^{-13}	4.83×10^{-13}	3.534×10^{-12}	1.76×10^{-14}
250	3.29×10^{-13}	7.219×10^{-13}	5.71×10^{-13}	3.243×10^{-12}	2.31×10^{-14}
300	4.05×10^{-13}	9.418×10^{-13}	6.84×10^{-13}	3.276×10^{-12}	3.08×10^{-14}
350	5.01×10^{-13}	1.194×10^{-12}	8.24×10^{-13}	3.461×10^{-12}	4.13×10^{-14}
400	6.22×10^{-13}	1.480×10^{-12}	9.92×10^{-13}	3.738×10^{-12}	5.53×10^{-14}
500	9.48×10^{-13}	2.147×10^{-12}	1.42×10^{-12}	4.477×10^{-12}	9.66×10^{-14}
600	1.41×10^{-12}	2.943×10^{-12}	2.01×10^{-12}	5.399×10^{-12}	1.61×10^{-13}
800	2.88×10^{-12}	4.920×10^{-12}	3.72×10^{-12}	7.690×10^{-12}	3.93×10^{-13}
1000	5.28×10^{-12}	7.409×10^{-12}	6.36×10^{-12}	1.052×10^{-11}	8.20×10^{-13}
1500	1.72×10^{-11}	1.586×10^{-11}	1.82×10^{-11}	1.982×10^{-11}	3.24×10^{-12}
2000	4.05×10^{-11}	2.752×10^{-11}	3.99×10^{-11}	3.225×10^{-11}	8.51×10^{-12}

[a] Calculated from $k = 6.39 \times 10^{-18} T^2 e^{(148/T)}$. [b] Calculated from $k = 6.18 \times 10^{-18} T^2 e^{(532/T)}$.

from ethanol is the longest and the C–H distance the shortest. For the H_β-abstraction the opposite is true; the C–O is the shortest and, correspondingly, the C–H is the longest. These findings indicate that the TS of the H_α-abstraction from ethanol occurs the earliest along the reaction coordinate and that of the H_β-abstraction the latest. The TS of the H-abstraction from methanol is between these two limits. This behavior is consistent with the Hammond postulate[29] that establishes a relationship between the proximity of the TS to the reactants and the exothermicity of the reaction. The H_α-abstraction in ethanol is the most exothermic and has the lowest energy of activation (see below); the H_β-abstraction is the least exothermic and has the highest energy of activation. It also indicates that the mechanism of H-abstraction is a one-step process without any accumulation of intermediates along the reaction coordinate.

An interesting difference is also observed between the structures of the transition states for H_α-abstraction (either in methanol or ethanol) and the H_β-abstraction in ethanol. The hydroxyl radical prefers to abstract a hydrogen in a gauche orientation with respect to the plane formed by the atoms C_2–O_1–H_1 (C_4–C_2–O_1 in H_β-abstraction from ethanol). The orientation of the hydroxyl radical interacting with H_α either in methanol or in ethanol is determined by the dipolar interaction between the O–H bonds and the lone pairs on the oxygens. In contrast, the orientation of the hydroxyl radical in the H_β-abstraction is determined by a hydrogen bond between the H of the hydroxyl radical and the lone pair on O_1 in the β^{I} structure, or the H of the hydroxyl group of ethanol and the oxygen of the hydroxyl radical in β^{II} structure. The O–H hydrogen bonding distances are shown in Figure 2, a and b, and the O–H–O angles in Table II.

B. Kinetics of H Abstraction. The values in Tables I and II have been used to calculate energy barriers (both forward and reverse corrected and uncorrected for ZPE), rate constants from classical transition state theory, k(TSTSYM), and the zero curvature approximation of the tunneling corrections to the rate constant, Γ^* (see Methods). The product of Γ^* and k(TSTSYM) is the tunneling corrected rate constant for the indicated reaction, and is denoted k(TSTSYM/ZCG-0). The above quantities were calculated for the H_α-abstraction from both methanol and ethanol, and for the H_β-abstraction from ethanol. The results are shown in Table III together with experimental values.

The rate constants calculated with the classical transition state theory, k(TSTSYM), are underestimated by comparison with the experimental values. For example, the calculated rate constant using HF/6-31G geometries and barriers determined at the highest computational level (MP4SDQ/6-311G**) is too small by a factor of 23 for H-abstraction from methanol. The rate constant for H_α-abstraction from ethanol at the similar computational level is underestimated by a factor of 5.0. As this discrepancy indicates, the low mass of the hydrogen atom necessitates the inclusion of tunneling in the calculation of the rate constants. Tunneling correction factors, Γ^*, and corrected rate constants, k-(TSTSYM/ZCG-0), are given in Table III. As expected, the tunneling correction increases the rate constants. The correction factor for the rate constant of H-abstraction from methanol is 10.04, and the correction for ethanol is only 1.04 because of the small forward barrier for the H_α-abstraction from ethanol. Consequently, the large discrepancy between the calculated uncorrected rate constants and the experimental values is reduced by the tunneling correction. The corrected rate constants are in good agreement with experiment, differing by factors of 2.3 and 4.8 for methanol and ethanol, respectively.

At the same level of computation (MP4SDQ/6-311G**) for the structure optimized at MP2, the uncorrected rate constant for H-abstraction from methanol is underestimated by a factor of 4300. Even the large tunneling correction (45.853) does not bring the calculated rate constant to an acceptable level; the corrected rate constant is too small by a factor of 94. Given the better imaginary frequencies obtained for the MP2 optimized TS (see Table III), it is reasonable to attribute the larger barriers to the fact that at this computational level not all the correlation energy is recovered. It has been suggested[12] that the correlation energy in perturbation theory calculations can be scaled to reproduce experimental bond energies (the MPn–SAC method). If it is assumed that the same fraction of the correlation energy is not recovered at different regions of the potential energy surface, then the correlation energy of the transition state can be scaled by the same factor. This scale factor, defined as

$$\mathcal{F}_n = \frac{\Delta H_{react}(\mathrm{MPn}) - \Delta H_{react}(\mathrm{SCF})}{\Delta H_{react}(\mathrm{exp}) - \Delta H_{react}(\mathrm{SCF})}$$

was calculated for a set of different hydrogen dissociation reactions. The value of $\mathcal{F}_n$ depends on the basis set and the level of correlation energy evaluation. In this work the values of $\mathcal{F}_4$ at the MP4/6-311G** level were 0.88 and 0.81, respectively, for C–H and O–H bond dissociation energies. The $\mathcal{F}_2$ values at the MP2/6-31G* level were 0.66 and 0.67, respectively, for the same bonds. The MP4-SAC/6-311G** results are shown in Table III. Clearly, the barriers and the calculated rate constants calculated with the MP4-SAC method for the α-H-abstraction from methanol and ethanol are in much better agreement with experiment. The rate constants are underestimated by factors of 4.2 and 6.5 for methanol and ethanol, respectively. It is still surprising that the results obtained for the HF optimized structures with the same basis set (MP4/6-311G**) give such good results without the need to apply the MP4-SAC correction. Possibly these results reflect a cancellation of errors that yields good calculated rate constants.

The above analysis and the data presented in Table III apply to reaction rates at or near 300 K. Because of the importance of radical reactions, and in particular of H-abstraction by OH radicals, in combustion chemistry the kinetics of these processes have been studied over a wide range of temperatures. Table IV gives both experimentally measured and theoretically calculated rate constants over a wide temperature range. The experimental values shown in Table IV are calculated from a nonlinear least-squares fit of several experimental results to the equation

(29) Hammond, G. S. *J. Am. Chem. Soc.* **1955**, *77*, 334.

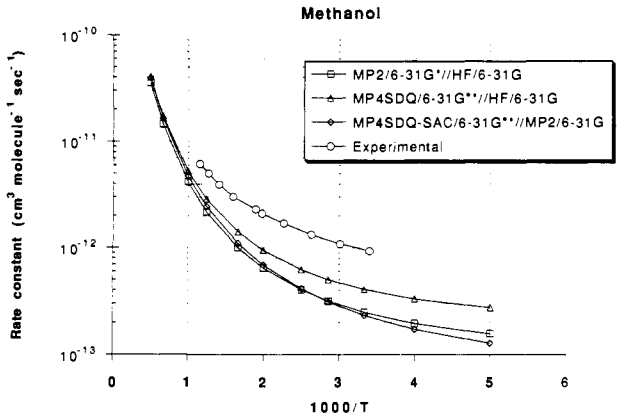

Figure 3. Comparison of calculated rate constants for H_α-abstraction from methanol at different levels of theory with experimental measurements[8] as a function of temperature.

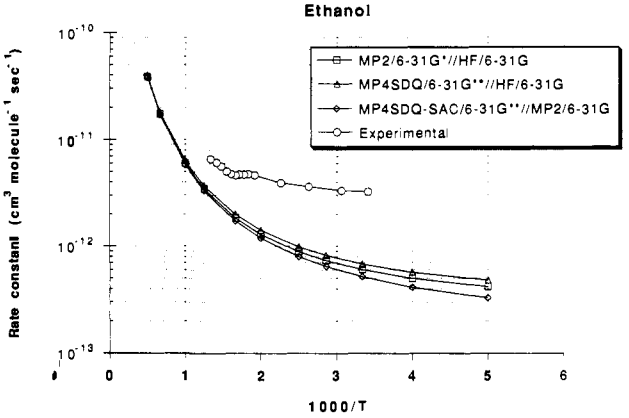

Figure 4. Comparison of calculated rate constants for H_α-abstraction from ethanol at different levels of theory with experimental measurements[31] as a function of temperature.

$k = CT^2e^{-D/T}$ reported by Atkinson.[30] The calculated rate constants at different levels of theory for H-abstraction are plotted in Figure 3 for methanol and in Figure 4 for ethanol, along with the experimental results of Hess and Tully.[8,31] As can be seen from the figures and from Table IV, the calculated rate constants are consistently smaller than the experimental ones, but the agreement between experimental and theoretical results improves with increasing temperature for H_α-abstraction from both methanol and ethanol. Also, the best results are obtained at the MP4/6-311G** level of computation for structures optimized at the HF/6-31G level.

Overall, the results from the tunneling corrected quantum mechanical calculations with the extended basis set (6-311G**) and with the inclusion of correlation up to MP4SDQ are in reasonably good agreement with experiment. However, the fact that the calculated rate constants are consistently too low is cause for some concern. This fact can be rationalized in several ways. First, one must recall that, for methanol, the experimental rate constants also include contributions from abstraction of the hydroxyl hydrogen. Several estimates of the relative contribution of the two pathways lead to a fraction of 0.85 of C–H versus O–H abstraction at 298 K.[30] The most recent estimate by McCaulley et al.[32] for the fraction of k_{OH} out of the total rate constant is 15 ± 8% at 298 ± 2 K. In the case of H-abstraction from ethanol, the experimentally observed rate constant is a sum of H_α-, H_β-, and H_O-abstraction rates. Furthermore, at higher temperatures the reaction is further complicated by the regeneration of OH• from the decomposition of the β-hydroxyethyl radical produced by H_β-abstraction. Meier et al.[5,23] have estimated that, at 300 K, 75 ± 15% of the total rate is due to H_α-abstraction. At this temperature no values are given for H_β-abstraction, but it is estimated[31] that at 600 K the contribution from this channel is ca. 15%.

Another source of error is the zero-curvature approximation for the calculation of the tunneling correction employed here. Because H-abstraction is a process in which a light atom (H) is transferred between two heavy groups, the reaction path will show a considerable curvature.[33] Such a curvature will increase the tunneling correction because it will allow tunneling in more than one dimension. More elaborate tunneling schemes, which take into account the local curvature in the vicinity of the TS, would be more rigorous and should yield larger rate constants. Additional error is introduced in the calculations of the rate constants in this work through the use of a harmonic approximation for the low-frequency vibrations. These internal hindered rotations, which have a considerable extent of anharmonicity, can become at higher temperatures free rotors. As has been shown by Truong and Truhlar[11] for CH_4 + OH, a free rotor representation of the low frequency vibrations increases the rate consistent at 300 K by approximately a factor of 2.

Even for the medium size molecules presented here, calculations such as those described above become very expensive due to the large number of basis functions and the calculation of correlation up to MP4. Consequently, attempts to simulate similar reactions for molecular structures larger than methanol and ethanol, such as the sugar moiety of DNA, will be prohibitively large. It is desirable to examine the results from calculations with a smaller basis set and compare them with those obtained with the extended basis set. A similar basis set and the inclusion of correlation only up to MP2 will become very useful in calculations of H-abstraction from the sugar of DNA, a process responsible for the radical-induced strand breakage in nucleic acids. We chose to use the split valence basis set augmented with polarization functions on heavy atoms (6-31G*), and to include correlation energy only to second order. The same structures as above were used, i.e., those obtained from UHF/6-31G geometry optimizations. The results, shown in Table III and in Figures 3 and 4, demonstrate that the smaller basis set and the inclusion of correlation only up to MP2 yield reasonably good results, which are in agreement with those from the more extended basis set with correlation energy included up to MP4. At the MP2/6-31G* level, the value of the uncorrected energy barrier, ΔV_u^f, for methanol is higher by 0.62 kcal mol^{-1} than at the MP4/6-311G** level. This leads to a smaller value for k(TSTSYM) but also to an increase in tunneling. The tunneling factor, Γ^*, increases from 10.04 to 17.37. Thus, the corrected rate constant, k(TSTSYM/ZCG-0), is only underestimated by a factor of 3.9. A similar analysis of H_α-abstraction from ethanol shows that using the MP2/6-31G* level of theory results in a decrease of only 11.4% in the tunneling corrected rate constant when compared with the MP4/6-311G** values. Simpler schemes of calculation were also considered, but only at the MP2/6-31G* level were the activation energies and rate constants found to be satisfactory.

Because of the good agreement between the results from MP4/6-311G** and MP2/6-31G* calculations, only the latter was used to calculate the abstraction of H_β from ethanol. Because experimental data are not available for this process in the gas phase, these calculations can be considered as a prediction of the kinetic parameters of this reaction. The results are shown in the last columns of Table III and Table IV. The uncorrected rate constant for the H_β-abstraction is three orders of magnitude smaller than the one for the H_α-abstraction. The difference stems primarily from the much larger barrier for the β-abstraction, which is 3.74 kcal mol^{-1} larger than that for the α-abstraction. Consequently, the tunneling correction is very large, and the corrected rate constant for β-abstraction is only one order of magnitude smaller than that for the α-abstraction process. This would suggest

(30) Atkinson, R. *J. Phys. Chem. Ref. Data* **1989**, *Monograph 1*, 160–161.
(31) Hess, W. P.; Tully, F. W. *Chem. Phys. Lett.* **1988**, *152*, 183–189.
(32) McCaulley, J. A.; Kelly, N.; Golde, M. F.; Kaufman, F. *J. Phys. Chem.* **1989**, *93*, 1014.
(33) Bondi, D. K.; Connoer, J. N. L.; Garrett, B. C.; Truhlar, D. G. *J. Chem. Phys.* **1983**, *78*, 5981–5989.

Table V. Thermochemical Quantities: C–H and O–H Bond Dissociation Energies (kcal mol^{-1}) Calculated at Different Levels of Theory from HF/6-31G and MP2/6-31G (in Parentheses) Geometries[a]

	H–CH_2OH	H–$CH(CH_3)OH$	H–CH_2CH_2OH	H–OH
experiment[b]	94.00	93.00		118.00
theory				
MP4/6-311G**	90.60 (91.23)	89.92 (90.45)		106.75 (107.65)
MP2/6-31G*	85.66	84.52	91.67	101.53
mpsac-corrected theory[b]				
MP4-SAC/6-311G**	93.38 (94.08)	92.76 (93.36)		113.94 (114.98)
MP2-SAC/6-31G*	93.19	92.29	100.62	115.97

		ethanol	
	methanol	α-H	β-H
experiment[c]	−24.00	−23.00	
theory			
MP4/6-311G**	−16.15 (−16.42)	−16.83 (−17.20)	
MP2/6-31G*	−15.87	−17.01	−9.86
mpsac-corrected theory			
MP4-SAC/6-311G**	−20.56 (−20.90)	−21.18 (−21.62)	
MP2-SAC/6-31G*	−22.78	−23.68	−15.35

[a] Energies of reaction, ΔH_{react} (kcal mol^{-1}), for H-abstraction from methanol and ethanol calculated from the bond dissociation energies. [b] See text and refs 34–36. [c] See text and ref 12.

that the contribution from this process to the overall rate constant measured experimentally is only of the order of a few percent.

C. Thermochemical Quantities. Various thermochemical quantities can be calculated from the energies shown in Tables I and II. Bond dissociation energies can be used to calculate the heats of formation of various radicals as well as the enthalpies of the H-abstraction reactions. In Table V, the bond dissociation energies, calculated at different levels of theory, are compared with experimental values.[34-36] It is important to note that no data are available for the heat of formation of the β-hydroxyethyl radical, and these calculations can provide the first estimate of this value.

A comparison between the theoretical and experimental results in Table V clearly shows that the agreement is not satisfactory. But when the MPn-SAC correction is applied, the results of the calculations are in much better agreement with experiment. The MP4-SAC/6-311G** and the MP2-SAC/6-31G* values are shown in Table V.

Comparison of the C–H bond strengths (Table V) to the barriers for H-abstraction (Table III) shows that the two parameters exhibit the same rank order: the barrier for H-abstraction is higher for stronger C–H bonds. Such a behavior would suggest that the strength of the C–H bond has an important contribution to the barrier for H-abstraction. However, there exists also a correlation between the activation energies and the distances of approach of OH$^\bullet$ to the carbon atom from which it abstracts the hydrogen and the C–H stretch in the TS. Comparison between the structural data in Table II and the calculated barriers in Table IV shows that the C–O distance in the transition state is inversely proportional to the barrier; that is, the smaller the barrier for H-abstraction, the longer is the C–O distance. The opposite is true for the relationship between the stretched C–H bond and the size of the barrier, the lowest barrier requires the smallest stretch of the C–H bond. This relationship suggests that for low barriers the transition state occurs early, giving rise to a long C–O distance and a short stretch of the C–H bond. When the barrier increases, the transition state occurs later, at shorter C–O distances and longer C–H stretches. It seems, therefore, that while the determination of relative rate constants for abstraction would require an elaborate determination of transition state structure and energy, the rank order of the susceptibility of H-abstraction can be predicted based on the strength of the C–H bond. It is important to point out that such a prediction can be accomplished by performing calculations on the isolated reactants, avoiding the costly calculation of the TS structures in the reaction. The electronic determinants defined above, taken together with a steric accessibility parameter, can provide a reliable predictor for the susceptibility of a hydrogen to abstraction by OH$^\bullet$. Because the abstraction of various hydrogens on the 2-deoxy-D-ribose may be responsible for strand breakage in nucleic acids, such a predictor can become very useful.

Since the H-abstraction reactions can be considered as composed of the breaking of a C–H bond and the formation of an O–H bond, the values of the bond dissociation energies can be used to calculate the heats of the H-abstraction reactions. The experimental heat of reaction for the H-abstraction from methanol is −25.35 kcal mol^{-1} and that of the H_α of ethanol is −26.12 kcal mol^{-1}. The MP4-SAC values underestimate the heat of the reaction by nearly 5 kcal mol^{-1}; for methanol the calculated heat of reaction is −20.43 kcal mol^{-1} and for the H_α of ethanol it is −21.08 kcal mol^{-1}. The MP2-SAC values are closer to the experimental heats of reaction, the difference being less than 3 kcal mol^{-1}. For methanol the value is −22.65 kcal mol^{-1} and for the H_α of ethanol it is −23.58 kcal mol^{-1}. The MP2-SAC calculation of the heat of abstraction of H_β of ethanol yields a value of −15.18 kcal mol^{-1}. Considering the underestimated values for methanol and H_α of ethanol, we estimate the heat of H_β-abstraction to be near 18 kcal mol^{-1}. From the known heat of formation of ethanol, we can estimate the heat of formation of the β-hydroxyethyl radical to be −16.56 kcal mol^{-1}.

D. Electronic Properties of the TS Structure. To gain a better understanding of the mechanism by which the strength of the C–H bond determines the barrier to H-abstraction, we have studied the electronic structure of the TS complex with an MCSCF method. The MCSCF calculations were carried out on two different geometries of the complex along the reaction coordinate that describes the process of H-abstraction. One structure is the TS and the other is constructed from the TS structure by shortening the C–H bond distance from its value at the TS to 1.1 Å. This structure, denoted as BTS, was not optimized and is only used here to explore the dependence of the electronic structure on the C–H bond distance. The MCSCF wave function was constructed as a complete active space (CAS) expansion of three electrons in three orbitals. The three chosen orbitals were the σ_{C-H}, the open-shell orbital that is initially localized on the oxygen of the OH$^\bullet$, and the σ^*_{C-H}. The analysis of the MCSCF wave function shows that from the eight possible configurations in the CAS, only three have a significant contribution to the wave function. These configurations are the ground state configuration (denoted as 210), a configuration in which one electron was excited

(34) Alfassi, Z. B.; Golden, D. M. *J. Phys. Chem.* **1972**, *76*, 3314.
(35) Golden, D. M.; Benson, S. W. *Chem. Rev.* **1969**, *69*, 125.
(36) Wagman, D. D.; Evans, W. H.; Parker, V. B.; Schumm, R. H.; Bailey, S. M.; Halow, I.; Churney, K. L.; Nutall, R. L. Technical Notes 270-3, 270-4, 270-5, 270-6, 270-7, and 270-8; National Bureau of Standards: Washington, DC, 1968.

Table VI. Weight of the Configurations in the MCSCF Wave Function and Atomic Spin Population in the Process of H-Abstraction

	methanol		ethanol			
			α-abstraction		β-abstraction	
	BTS	TS	BTS	TS	BTS	TS
			Configurations[a]			
210	0.9872	0.9706	0.9878	0.9708	0.9874	0.9708
111	0.0054	0.0229	0.0049	0.0228	0.0054	0.0225
012	0.0063	0.0058	0.0063	0.0058	0.0062	0.0059
			Spin			
C	0.1304	0.4822	0.1254	0.4666	0.1358	0.5360
H	0.0382	0.0858	0.0364	0.0856	0.0378	0.0802
O	0.8946	0.5103	0.8979	0.5188	0.8944	0.4962

[a] The configuration 210 corresponds to the ground state; the 111 to a single excitation from σ to σ^*; and 012 to a double excitation from σ to σ^*.

from σ_{C-H} to σ^*_{C-H} (denoted as 111), and a configuration with a double excitation from σ_{C-H} to σ^*_{C-H} (denoted as 012). The change in the MCSCF wave function as the hydrogen moves from its position in the BTS geometry to that in the TS can be followed by the change in the square of the coefficients of the three configurations as shown in Table VI. Since the square of the coefficient is proportional to charge density, the changes reflect the redistribution of charge in the process of the approach of the hydrogen toward the TS geometry. The results presented in Table VI clearly indicate that by stretching the C–H distance toward the TS the square of the coefficient of the 111 configuration changes its value approximately by a factor of 4, while the other two configurations change much less. The singly excited 111 configuration in the doublet state is a representation of a system in which the C–H bonds has no contribution to bonding because one electron occupies the bonding σ orbital, one occupies the antibonding σ^*, and one is in the open shell orbital. Thus, the equal mixing of the bonding and antibonding orbitals in this configuration describes the process of breaking the C–H bond and provides an explanation for the correlation between the barrier and the strength of the C–H bond (see above). These conclusions are supported by the changes in the charge and spin populations (Table VI) that take place upon the formation of the TS. As expected, the spin in the structure **BTS** is localized on the oxygen of the hydroxyl radical. However, upon stretching the C–H bond to form the TS, approximately half of the spin is transferred from the oxygen to the carbon with virtually no spin transferred to the hydrogen. This is consistent with a three-center, three-electron bond in which the spin is localized on the end-atoms and the charge density is concentrated between the end-atoms and the central hydrogen. The charge shows a small degree of redistribution in the TS; the oxygen becomes more negative and the abstracted hydrogen more positive with values intermediate between an OH• and an O–H bond in water. This suggests that the charge redistribution reflects the partial breaking of the C–H bond and the concomitant partial formation of the O–H bond.

Similar conclusions have been reached based on a generalized valence bond (GVB) description of the bond breaking and making in two reactions.[37] $H_2 + D \rightleftarrows H + HD$ and $LiH + H \rightleftarrows Li + H_2$. The authors conclude that in a three-center exchange reaction, such as those considered here and in their work, the bonding orbital of the reactants changes smoothly to the bonding orbital in the product. At the same time, the orbital that contains the unpaired electron readjusts to remain orthogonal to the bonding orbital. Consequently, it changes phase as it shifts centers during the reaction, and at the **TS** the density from this orbital on the central H atom is nearly zero.

E. Consideration of the Effect of Solvent. It is interesting to compare the kinetic parameters of H-abstraction by OH• from methanol and ethanol in the gas phase to those in solution. In a pulse radiolytic study, Asmus et al.[38] measured the relative yields of H-abstraction from different atoms of aliphatic alcohols. In methanol, 93.0% of the total yield was due to abstraction of the hydrogen from C_α and 7.0% from the hydroxyl group. In ethanol, 84.3% was from C_α, 13.2% from C_β, and 2.5% from the hydroxyl group. Since the H-abstraction process is kinetically controlled, we can estimate the relative rate constants for H-abstraction from C_α and C_β of ethanol. The ratio is 6.4, which is considerably different from the ratio of ca. 20 obtained in the gas phase (see Table III). A possible way to rationalize this difference is through the effects of the solvent on the observed rate constants. Without conducting extensive molecular dynamics simulations of the process in solution, one can estimate the effect of the solvent by comparing the dipole moments of the **TS** for H-abstraction because the major solvation of these neutral molecules will depend on their dipole moment. The dipole moments of the TS of H_α-abstraction calculated with the 6-31G basis set are 1.103 and 1.552 D for methanol and ethanol, respectively. By comparison, the dipole moments of the two TS of the H_β-abstraction in ethanol are 4.639 and 2.885 D for β^{I} and β^{II}, respecively. Clearly, the larger dipole moment of the TS for the abstraction of H_β than that for the abstraction of the H_α of ethanol will contribute to a larger stabilization of the TS and will result in a smaller ratio of the rate constants than the one calculated in the gas phase. Because the stabilization is relative to the ground state, we also must compare the dipole moments of the TS with those of the separated molecules. The dipole moment, calculated with the 6-31G basis set, of OH• is 2.146 D, of methanol is 2.287 D, and of ethanol is 2.069 D. Thus, while the transition states for the abstraction of H_α of methanol and ethanol are *less* polar than the separated reactants, the transition state for the abstraction of H_β is *more* polar than the separated reactants. In other words, the relative effect of the aqueous solvent will be to facilitate the H_β-abstraction and to slow down the abstraction of H_α. It is difficult to estimate this effect *quantitatively* without conducting molecular dynamics simulations of this process in aqueous solution.

Acknowledgment. We indebted to Harel Weinstein for his careful reading of the manuscript and many helpful comments and suggestions. This research was supported in part by U.S. Department of Energy Grant DE-FG02-88ER60675. A generous grant of computer time from the University Computer Center of the City University of New York is gratefully acknowledged. We also thank the National Energy Research Supercomputer Center at Lawrence Livermore National Laboratory for providing computer time to perform some of the calculations in this work.

Registry No. CH_3OH, 67-56-1; CH_3CH_2OH, 64-17-5; OH, 3352-57-6; CH_2OH, 2597-43-5; CH_3CHOH, 2348-46-1; CH_2CH_2OH, 4422-54-2; H_2O, 7732-18-5.

(37) Goddard, W. A., III; Ladner, R. C. *J. Am. Chem. Soc.* **1971**, *93*, 6750–6756.

(38) Asmus, K.-D.; Mockel, H.; Henglein, A. *J. Phys. Chem.* **1973**, *77*, 1218–1221.